A SUPER-RESOLUTION NEAR-FIELD SCATTERING CENTERS EXTRACTION METHOD FOR SPHERICAL WAVEFRONT CURVATURE COMPENSATION

W. D. Hu*, R. Liu, C. Wu, and C. Y. Shi

Beijing Institute of Technology, No. 5 South Street, Zhongguancun, Haidian District, Beijing 100081, China

Abstract—While a radar target is illuminated under the condition of spherical wave, two-dimensional ISAR image can be obtained in near field, and the wavefront curvature must be compensated. A novel two-dimensional mathematical model is set up, and a 2D-ESPRIT super-resolution algorithm based on matrix pencil is applied to estimate the accurate locations of the scattering centers in near field. Numerical simulations are conducted in different distances as well as with different SNRs. It is proved that the method can revise the spherical wavefront curvature with a high accuracy. Finally, near field ISAR imaging experiments were done outdoor, and raw data were processed with this super-resolution method, which verify that 2D-ESPRIT algorithm based on matrix pencil can compensate the spherical wavefront curvature effectively in near field.

1. INTRODUCTION

High-resolution radar techniques have led to much more advanced radar capabilities in gathering information on the fine features of a target. Radar targets imaging is of great value for multiple scattering centers extraction and characteristics measurements [1]. Conventionally, two-dimensional imaging has been implemented in far field. Nevertheless, targets will be illuminated by spherical wave in many cases, which is so called near field imaging. So spherical wavefront curvature must be compensated in precise measurements.

In last two decades, some procedures have been developed to deal with this problem. The wavefront curve is presented in near field in [2].

A planar near-field measurement for far-field RCS determination is presented in [3]. Spherical wave near-field radar imaging techniques are used to extract far-field RCS in [4]. High order ESPRIT method is used to estimate near filed source in [5]. The fast cyclical convolution is firstly used for computing the near-field image in [6]. However, there exist some errors for all kinds of methods.

In the same time, super-resolution algorithms, especially Esprit methods, have been widely used in estimations of directions of arrival [7–9]. It also can be applied to the estimation of scattering centers. In this paper, a new mathematical model is set up for near-field ISAR imaging. A 2D-ESPRIT super-resolution algorithm based on matrix pencil is applied to estimate the accurate location of near-field multiple scattering centers. Numerical simulation is conducted under variable distance condition, and three extinguishers imaging experiment is done outdoor. Both prove that this method can revise the near-field problem effectively.

2. MATHEMATICAL MODEL OF SPHERICAL WAVE IMAGING

The geometry of the turntable target imaging is illustrated in Fig. 1, in which a target consists of independent and non-directional scattering centers, and its scattering reflectivity is $g(x, y)$ with coordinate (x, y). After it is rotated by a scan angle θ, the coordinate is changed to (u, v). The imaging radar is located in the near field of the target, so there exits spherical wavefront curvature. The measurement waveform is supposed stepped frequency signal, and the wide effective bandwidth can result in high range resolution.

Suppose that $g(x, y)$ is the scattering function of a target. The relation of the coordinates (u, v) and (x, y) is

$$\begin{cases} u = x \cos \theta + y \sin \theta \\ v = -x \sin \theta + y \cos \theta \end{cases} \tag{1}$$

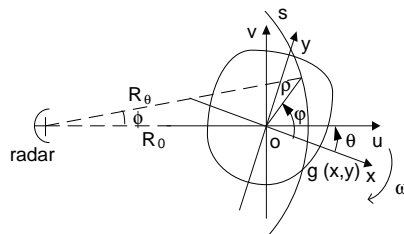**Figure 1.** Geometrical parameters of the turntable situation.

$$\begin{cases} x = u\cos\theta - v\sin\theta \\ y = u\sin\theta + v\cos\theta \end{cases} \tag{2}$$

The scattered field $z(k,\theta)$ can be given by:

$$z(k,\theta) = \iint\limits_{D} g(x,y)\frac{\exp(-j2\pi k R_\theta)}{R_\theta^2}dxdy \tag{3}$$

In this formula, there is

$$R_\theta = \sqrt{(R_0+u)^2+v^2} = \sqrt{R_0^2+\rho^2+2R_0\rho\cos(\varphi-\theta)} \tag{4}$$

and R_0 is the range from the radar antenna to the rotation center. $k = 2f/c$ is the spatial frequency, $f = f_0 + n\Delta f$, and Δf is the frequency step.

R_θ can be represented by Taylor series

$$R_\theta \approx R_0 + \rho\cos(\varphi-\theta) + \frac{\rho^2\sin^2(\varphi-\theta)}{2[R_0+\rho\cos(\varphi-\theta)]}$$

$$= R_0 + x\cos\theta + y\sin\theta + \frac{(y\cos\theta - x\sin\theta)^2}{2(R_0+x\cos\theta+y\sin\theta)} \tag{5}$$

According to the condition of small angle in ISAR imaging, here R_θ can be simplified as

$$R_\theta = R_0 + x + y\theta + \frac{y^2 - 2xy\theta}{2(R_0+x)} \tag{6}$$

It can be deduced step by step

$$R_\theta^2 \approx \left(R_0 + x + \frac{y^2}{2R_0+2x}\right)^2 \tag{7}$$

If the radar signal is step frequency signal, there is

$$k = k_0 + n\Delta k \ (\Delta k \ll k_0), \quad n = 0,1,\ldots N-1.$$
$$\theta = m\Delta\theta, \quad m = 0,1,\ldots M-1.$$

suppose that there are p scattering points, $p < m$, $p < n$, the scattering function can be represented by Taylor series as

$$z(n\Delta k, m\Delta\theta) = \sum_{p=0}^{P-1} g(x_p,y_p)\Delta x\Delta y / \left(R_0 + x_p + \frac{y_p^2}{2R_0+2x_p}\right)^2$$

$$\cdot \exp[-j2\pi(k_0+n\Delta k)R_0] \cdot \exp\left[-j2\pi(k_0+n\Delta k)\right.$$

$$\left.\cdot\left(x_p + \frac{y_p^2}{2R_0+2x_p}\right)\right] \cdot \exp\left[-j2\pi k_0 m\Delta\theta\left(y_p - \frac{x_p y_p}{R_0+x_p}\right)\right] \tag{8}$$

This is the near-field two-dimensional imaging mathematical model.

3. 2D-ESPRIT ALGORITHM BASED MATRIX PENCIL

Based on the two-dimensional imaging mathematical model, super-resolution methods are taken into account to deal with the near-field scattering centers extraction. A 2D-ESPRIT algorithm has the capability of wavefront compensation while spherical wave illuminating.

We can suppose these functions as

$$z'(n,m) = z(n\Delta k, m\Delta\theta)\exp[j2\pi(k_0 + n\Delta k)R_0]$$

$$x'_p = x_p + \frac{y_p^2}{2R_0 + 2x_p}, \quad y'_p = y_p - \frac{x_p y_p}{R_0 + x_p} \tag{9}$$

So (8) can be changed to

$$z'(n,m) = \sum_{p=0}^{P-1} g(x_p, y_p)/(R_0 + x'_p)^2 \cdot \exp\left(-j2\pi k_0 x'_p\right)$$

$$\cdot \exp\left(-j2\pi n\Delta k x'_p\right) \cdot \exp\left(-j2\pi k_0 m\Delta\theta y'_p\right) \tag{10}$$

There exists a stable phase between these matrices,

$$z'(n,m), \ z'(n+1,m), \ z'(n,m+1)$$

Now three subspace matrices X, Y, Z can be divided from the original data matrix.

According to the theory of Esprit algorithm, there exists this formula

$$\begin{cases} X = AS + N_x \\ Y = A\Phi S + N_y \\ Z = A\Theta S + N_z \end{cases} \tag{11}$$

X, Y, Z are $(N-1) \times (M-1)$ dimensional matrices. A is $(N-1) \times (M-1) \times P$ dimensional matrix. N_i $(i = x, y, z)$ is measured noise matrix, and there are relations as follows:

$$\begin{cases} A(n,m,p) = \exp[-j2\pi(k_0 + n\Delta k)x'_p] \cdot \exp(-j2\pi k_0 m\Delta\theta y'_p) \\ S = [g(x_0, y_0)/(R_0 + x'_0)^2, g(x_1, y_1)/(R_0 + x'_1)^2, \\ \qquad \ldots, g(x_P, y_P)/(R_0 + x'_P)^2] \\ \Phi = \text{diag}(\exp(-j2\pi\Delta k x'_0), \exp(-j2\pi\Delta k x'_1), \\ \qquad \ldots, \exp(-j2\pi\Delta k x'_P)] \\ \Theta = \text{diag}(\exp(-j2\pi k_0\Delta\theta y'_0), (\exp(-j2\pi k_0\Delta\theta y'_1), \\ \qquad \ldots, (\exp(-j2\pi k_0\Delta\theta y'_P)] \end{cases} \tag{12}$$

The matrices A and S are not rank deficient by assumption. The matrices Φ and Θ are diagonal and contain phase shift information of scattering centers, and the accurate location of every scattering center can be estimated.

Two new matrices can be constructed by X, Y and Z data matrices. Singular values decomposition is done, and the SVDs of two matrices are computed.

$$\begin{bmatrix} XYZ \end{bmatrix} = U_1 D_1 V_1^H \quad \begin{bmatrix} X \\ Y \\ Z \end{bmatrix} = U_2 D_2 V_2^H \tag{13}$$

where U and V are unitary matrices. D is a diagonal matrix containing the eigenvalues, and H denotes Hermitian conjugation. The TLS approximation of the data matrices share the same column space range of $\hat{U}_1$ and row space range of $\hat{V}_2$, and are obtained by X, Y, Z onto these subspaces:

$$\begin{cases} E_x = \hat{U}_1^H X \hat{V}_2 \\ E_y = \hat{U}_1^H Y \hat{V}_2 \\ E_z = \hat{U}_1^H Z \hat{V}_2 \end{cases} \tag{14}$$

Now, we can define:

$$E_\varphi = E_x^{-1} E_y, \quad E_\theta = E_x^{-1} E_z$$

From this set of equations, the eigenvalues of E_φ and E_θ need to be computed. It is clear that they share, in the noise free case, the same set of eigenvectors, which means that they can be tri-angularized by the same unitary matrix Q. There exists the unitary matrix Q such that

$$Q^H E_\varphi Q = T_\varphi, \quad Q^H E_\theta Q = T_\theta$$

Here the upper triangular matrices T_φ, T_θ have main diagonals with regard to Φ and Θ, respectively. Suppose that there are p scattering centers of the target, φ_p and θ_p are preserved in the positions corresponding to the diagonals, and no pair matching operation needs to be done.

$$\begin{cases} x_p' = \frac{\varphi_p}{-2\pi \Delta k} \\ y_p' = \frac{\theta_P}{-2\pi k_0 \Delta \theta} \end{cases} \tag{15}$$

According to this 2D-ESPRIT algorithm, the locations of the scattering centers are estimated effectively. Because the spherical wave mathematical model has been applied to this algorithm, near-field effect can be revised at the same time.

4. NUMERICAL SIMULATION

To verify the method discussed in the previous section, a numerical model is set up, which is composed of six scattering centers, and their coordinates are A(2,2), B(3,3), C(4,4), D(5,5), E(6,6), F(7,7). All the

values of their scattering strength are 0 dBm. The SNR is supposed as 20 dB. The rotating center locates in O(0,0).

The carrier frequency of the imaging radar is 35 GHz. The step frequency is 2 MHz. The accumulating angle is 3 degree. Both M and N are 128. The total bandwidth is 256 MHz. According to the classical far field condition, the distance of plane wave illumination is 33600 meters.

Now, we chose the distances of 100 meters, 50 meters and 30 meters. The spherical wavefront curvature can be simulated and demonstrated in Figs. 2, 3 and 4. At the same time, the wavefront curvature is compensated by 2D-ESPRIT imaging algorithm.

When the measurements range is 100 meters, the spherical image of six scattering centers is shown using six "cross" in Fig. 2(a). The image of six scattering centers in far filed is shown using six "circle". It can be seen that the wavefront curvature is very clear. The point F(7,7) is changed to the coordinate of (6.546, 7.224). After processing with 2D-ESPRIT algorithm, the deviation is compensated as in Fig. 2(b).

When the measurements range is 50 meters, the deviation of curvature is larger than that in 100 meters. The image of six scattering centers is shown using six "cross" in Fig. 3(a). The point F(7,7) is changed to the coordinate of (6.091, 7.395). The difference will be apparent. After processing with 2D-ESPRIT algorithm, the deviation is compensated as in Fig. 3(b).

When the measurements range is changed to 30 meters, the deviation of curvature is clearer. The image of six scattering centers is
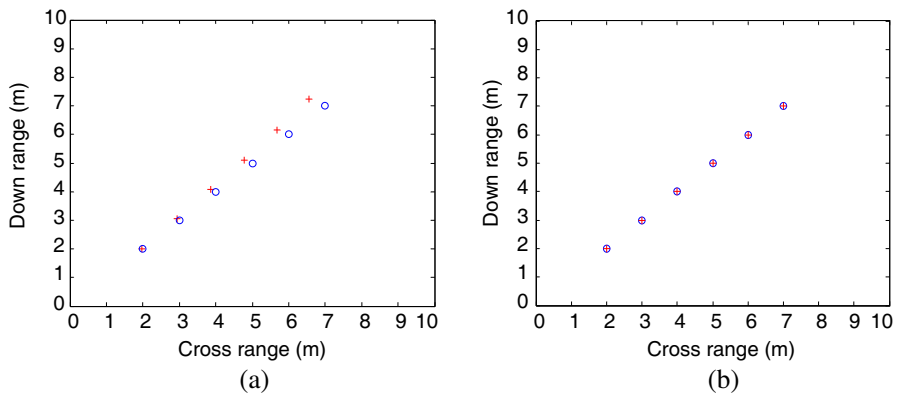

Figure 2. Comparison of spherical-wave compensation effect of six points in 100 m. (a) Spherical-wave image and far-field image in 100 m. (b) Spherical-wave compensation image in 100 m.

shown using six "cross" in Fig. 4(a). The point F(7,7) is changed to the coordinate of (5.596, 7.659). The difference will be very apparent. After processing with 2D-ESPRIT algorithm, the deviation is compensated as in Fig. 4(b).

Of course, signal-noise-rate is of great importance to this algorithm. Suppose that the measurement distance is 100 meters. When SNR is 5 dB, 10 dB and 12 dB, the location estimation accuracy will be different. It can be explained with Fig. 5 and Table 1.
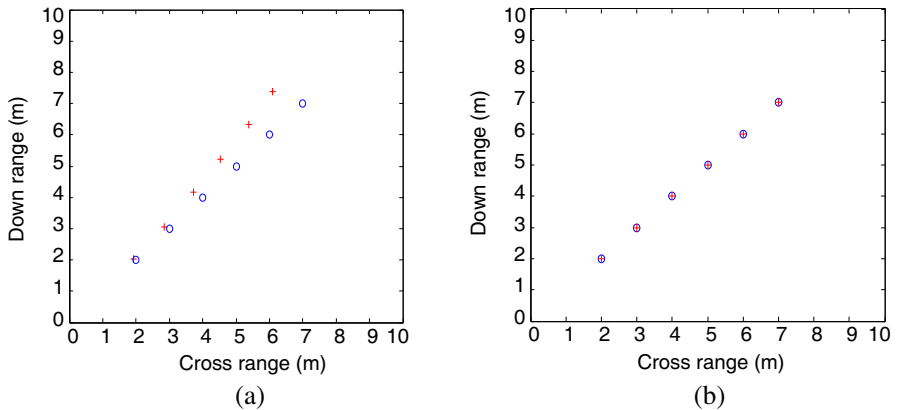

Figure 3. Comparison of spherical-wave compensation effect of six points in 50 m. (a) Spherical-wave image and far-field image in 50 m. (b) Spherical-wave compensation image in 50 m.
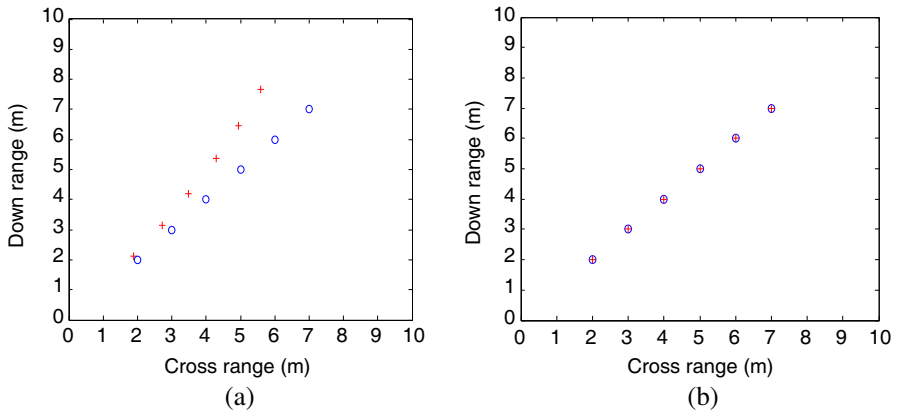

Figure 4. Comparison of spherical-wave compensation effect of six points in 30 m. (a) Spherical-wave image and far-field image in 30 m. (b) Spherical-wave compensation image in 30 m.
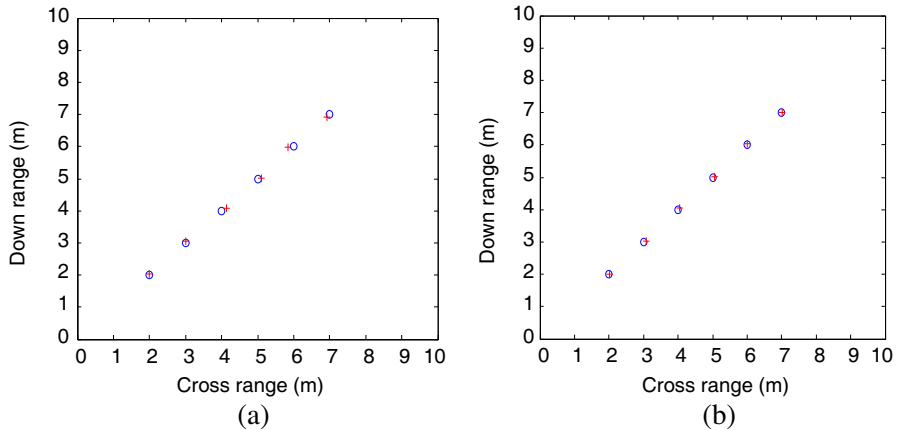
Figure 5. Comparison of scattering centers estimation with different SNR. (a) Six scattering centers estimation when SNR = 5 dB. (b) Six scattering centers estimation when SNR = 12 dB.

Table 1. The location estimation values of six scattering points with different SNR.

SNR		A	B	C	D	E	F	deviation
5 dB	x	1.9887	3.0156	4.1360	5.0939	5.8411	6.9330	0.1589
	y	2.0400	3.0603	4.0850	5.0252	5.9703	6.9291	
10 dB	x	2.0145	3.0148	4.0559	5.0067	5.9647	6.9690	0.0688
	y	2.0688	3.0523	4.0625	5.0541	5.9973	7.0581	
12 dB	x	2.0064	3.0469	4.0435	5.0468	6.0020	7.0152	0.0502
	y	2.0003	3.0360	4.0502	5.0235	6.0325	7.0060	

In Table 1, the locations of six scattering centers A(2,2), B(3,3), C(4,4), D(5,5), E(6,6), F(7,7) are estimated with 2D-ESPRIT algorithm with different SNRs. x is the crossrange, and y is the downrange. The deviations all can be obtained with different SNRs.

According to these comparisons, when SNR is supposed to be 5 dB, the location deviation is 15.89% of the measurement distance; when SNR is equal to 10 dB, the deviation is 6.88% of the distance; and when SNR is 12 dB, the deviation accuracy is 5%, thus, we think that it is can be accepted in experiments.

The deviation can be shown in Fig. 5, the same as in Table 1. When SNR is 12 dB, the location deviation is not apparent, but

Figure 6. Three extinguishers on a rotator outdoor.

suppose that it is 5 dB, the deviation is larger.

It can be seen from these comparisons, the spherical wavefront curvature is distinct as the range is reduced. Whatever the distance is, only if the SNR is larger than 12 dB, the 2D-ESPRIT imaging algorithm can compensate the spherical wave effect entirely with a high accuracy.

5. EXPERIMENTAL RESULTS

The experiment is executed outdoor. There is a big rotator, on which three extinguishers are set as Fig. 6. Suppose that the rotator center locates in O(0, 0). The coordinate of three extinguishers are O(0, 0), P(4.6, 3.8), Q(−4.6, −3.8). The measurements radar is 100 meters from the center of the rotator. The carrier frequency of the radar is 35 GHz. The step frequency is 2 MHz. The accumulating angle is 3.4 degree. Both M and N are 128. The total bandwidth is 256 MHz.

Three extinguishers on the rotator are shown in Fig. 6. Traditionally, the convolution back-projection algorithm is often used to spherical wave imaging, but the wavefront curvature cannot be revised entirely. The 2-D images of three extinguishers are illustrated in Fig. 7(a). When 2D-ESPRIT algorithm is applied to the real data sets, compared with the CBP results, the deviation can be demonstrated in Fig. 7(b). Three "cross" image shows the result of CBP method, and three "circle" image shows the result of 2-D ESPRIT method.

The image of three extinguishers is shown in Fig. 7(a). The coordinate values of these scattering centers can be extracted. P locates in (−4.48, −3.75); O locates in (−0.14, −0.07); and Q locates in (4.41,3.86). They can also be shown using three "cross" in Fig. 7(b). The image of 2D-ESPRIT processing is shown using three "circle" in this figure. It is proved by experiment that the spherical wavefront curvature appears while using CBP method, and 2D-ESPRIT method can compensate the curvature effectively.
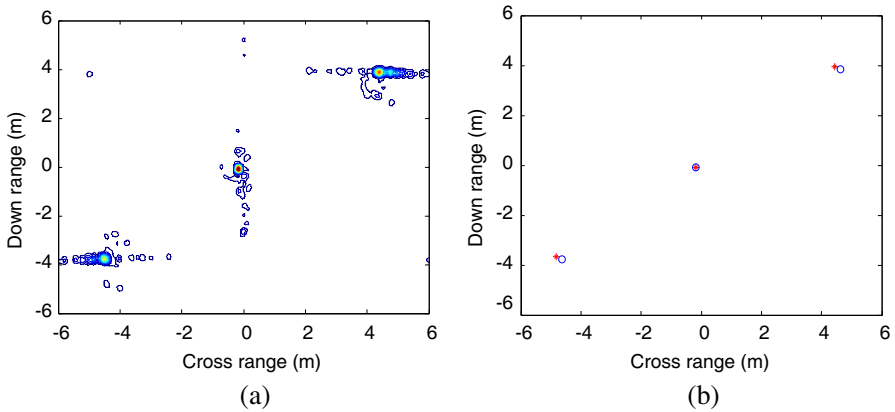
Figure 7. Comparison of spherical-wave compensation effect of three extinguishers image in 100 m. (a) Three extinguishers image using CBP. (b) Three extinguishers images using CBP and ESPRIT.

6. CONCLUSION

Two-dimensional ISAR image is easy to be obtained under far field condition, but a target is often radiated by spherical wave, which is near field imaging. CBP algorithm is used to give the ISAR image, but the wavefront curvature cannot be compensated. The key of 2D-ESPRIT algorithm applied in ISAR imaging is the building of a novel two-dimensional mathematical model. Based on this, the 2D-ESPRIT super-resolution algorithm is used to estimate the accurate locations of the scattering centers in near field. Numerical simulations are conducted in 100 meters, 50 meters and 30 meters. It is obvious that the spherical wavefront curvature is larger with shorter distance, only if the 2D-ESPRIT method is used with enough SNR as 12 dB. The compensation accuracy will be 5% of the measurement distance. Finally, near field ISAR imaging experiments were done outdoor. Raw data have been processed with this super-resolution method, which verify that the 2D-ESPRIT algorithm based on matrix pencil can compensate the spherical wavefront curvature effectively in near field.

REFERENCES

1. Mensa, D. L., *High Resolution Radar Cross Section Imaging*, 458–462, Artech House, London, Boston, 1991.

2. Li, H.-J. and F.-L. Lin, "Near field imaging for conducting objects," *IEEE Trans. Antennas Propag.*, Vol. 39, No. 5, 600–605, 1991.

3. LaHaie, I. J., E. I. L. Baron, and J. W. Burns, "Far field radar cross-section (RCS) predictions from planar near field measurements," *IEEE AP-S Symp. Dig.*, 1542–1545, Chicago, 1992.

4. Broquetas, A., "Spherical wave near-field imaging and radar cross-section measurement," *IEEE Trans. Antennas Propag.*, Vol. 46, No. 5, 730–735, 1998.

5. Yuen, N. and B. Friedlander, "Performance analysis of higher order ESPRIT for localization of near-field sources," *IEEE Trans. Signal Processing*, Vol. 46, No. 3, 709–719, 1998.

6. Vaupel, T. and T. F. Eibert, "Comparison and application of near-field ISAR imaging techniques for far-field radar cross section determination," *IEEE Trans. Antennas Propag.*, Vol. 54, No. 1, 144–151, 2006.

7. Haardt, M., R. N. Challa, and S. Shamsunder, "Improved bearing and range estimation via high-order subspace based Unitary ESPRIT," *Proc. 30th Asilomar Conference on Signals, Systems and Computers*, Vol. 1, 380–384, 1996.

8. Van der Veen, A. J., P. B. Ober, and E. F. Deprettere, "Azimuth and elevation computation in high resolution DOA estimation," *IEEE Trans. Signal Processing*, Vol. 40, No. 7, 1828–1832, 1992.

9. Van der Veen, A. J. and E. F. Deprettere, "Parallel VLSI matrix pencil algorithm for high resolution direction fingding," *IEEE Trans. Signal Processing*, Vol. 39, No. 2, 383–394, 1991.

10. Li. H.-J., N. H. Farhat, et al., "Image understanding and interpretation in microwave diversity imaging," *IEEE Trans. Antennas Propag.*, Vol. 37, No. 8, 1048–1057, 1989.

11. Peixoto, G. G., M. A. Alves, I. M. Martin, M. C. de Rezende, and A. Medium, "A medium open range radar cross section facility in Brazil," *PIERS Online*, Vol. 5, No. 4, 381–384, 2009.

12. Martin, I. M., M. A. Alves, G. G. Peixoto, and M. C. Rezende, "Radar cross section measurements and simulations of a model airplane in the X-band," *PIERS Online*, Vol. 5, No. 4, 377–380, 2009.